time span simulated (fig. S6 and table S8). These results, combined with the lack of resolution within superclades of the metazoan tree, argue against models of metazoan radiation in which the temporal window of diversification is much larger (*48*).
39. J. A. Clack, *Gaining Ground: the Origin and Evolution of Tetrapods* (Indiana Univ. Press, Bloomington, IN, 2002).
40. N. Takezaki, F. Figueroa, Z. Zaleska-Rutczynska, N. Takahata, J. Klein, *Mol. Biol. Evol.* **21**, 1512 (2004).
41. Y. I. Wolf, I. B. Rogozin, E. V. Koonin, *Genome Res.* **14**, 29 (2004).
42. J. E. Blair, K. Ikeo, T. Gojobori, S. B. Hedges, *BMC Evol. Biol.* **2**, 7 (2002).
43. H. Philippe, N. Lartillot, H. Brinkmann, *Mol. Biol. Evol.* **22**, 1246 (2005).
44. S. L. Baldauf, J. D. Palmer, *Proc. Natl. Acad. Sci. U.S.A.* **90**, 11558 (1993).
45. J. L. Boore, D. Lavrov, W. M. Brown, *Nature* **393**, 667 (1998).
46. A. Rokas, P. W. H. Holland, *Trends Ecol. Evol.* **15**, 454 (2000).
47. A goodness-of-fit test using parametric bootstrapping (*15*) showed that even the best-fit model of sequence evolution does not adequately describe the evolution of the sequence data from these 32 fungal and metazoan taxa (fig. S8).
48. G. A. Wray, J. S. Levinton, L. H. Shapiro, *Science* **274**, 568 (1996).
49. We thank D. Arendt for providing RNA for *Platynereis dumerilii;* C. Ané for providing the modified version of the Seq-Gen simulation software with an implementation of a covarion model; and B. Prud'homme, B.

Table 2. Experimental schemes and determined absorption coefficient β (cm^{-1} $torr^{-1}$), the percentage of enrichment or depletion (negative values) at a pressure of 1 torr for a 3-min separation period, and pressure dependence of conversion rate $\gamma = kp + y$ of C_2H_4 at a temperature of 300 K, where k, p, and y are in units of s^{-1} $torr^{-1}$, torr, and s^{-1}, respectively. Rovibrational transition is from the ground state to the $\nu_7 = 1$ state. Frequency offset Δf denotes the C_2H_4 transition d3 2-298.0276 4J/F43756.0

the symmetry representations correspond to even or odd parity of an energy level.

We now report the successful use of LID to deplete the population of the B_{2u} isomer in a sample of gaseous ethylene, followed by monitoring of the subsequent spin conversions for the return to equilibrium. We measured isomer concentrations by recording the absorption intensities of spectral lines with appropriate J, K_a, and K_c quantum numbers. Our experimental setup uses two CO_2 lasers (Edinburgh Instruments PL3 as the separation laser and a home-built laser as the probe) and three glass cells (for separation, test, and reference) (*16*). We measured the spin conversion rates for $^{13}CH_3F$ with this setup and obtained good agreement with the published results (*6*, *7*).

For the ethylene study, the experimental schemes are shown in Table 2, where the reported results from high-resolution infrared spectroscopy (*17*) were used to calculate the frequency offsets between the C_2H_4 transition frequencies and the CO_2 laser frequencies. Application of the LID technique for the separation of nuclear spin isomers requires that a molecular transition be near-coincident with a CO_2 laser line. Here, the 10*P*44 laser line with a power of 6 W was used. Its frequency was tuned about 20 MHz above the center frequency by adjusting the laser cavity length to set it in the red wing of the $9_{0,9} \leftarrow 10_{1,9}$ line of the ν_7 band of ethylene. This frequency selectively excited the B_{2u} isomer, with the other three isomers acting as a buffer gas. The B_{2u} molecules drift, by the LID effect, along the direction of the separation laser beam in the separation cell, thereby depleting the B_{2u} species and enriching the A_g, B_{1g}, and B_{3u} species at the entrance end of the cell; this direction of drift corresponds to an increase in the collision cross section upon excitation. The nonequilibrium population was then transferred through a valve from the near end of the separation cell to the test cell. For high sensitivity, we measured differential absorption by splitting the probe beam to acquire simultaneous data from the test cell and the reference cell with a population at thermal equilibrium. We determined normalized absorption intensity differences for appropriate probe lines to observe the initial degree of isomer depletion or enrichment. At an ethylene pressure of 1 torr, the probe was tuned through five absorption lines belonging to one of the species B_{2u}, B_{3u}, or A_g (cases 1 to 5 in the seventh column of Table 2 together with the corresponding absorption coefficients in the sixth column) (*18*). The depletion of the B_{2u} species was about 3%, with 1% or less enrichment of the other three isomers.

The equilibration kinetics of the B_{2u}-depleted sample were measured as follows: For the first 1-min period, the separation laser was blocked and the valve was kept open to record the zero baseline of the differential signal in the first period. Then, in the second period, the separation laser was unblocked and its beam was introduced into the separation cell for 3 min to generate the nonequilibrium distribution in the test cell. Then the valve was closed, and the decay curves due to isomeric conversion were monitored during the third period. Typical signals are shown for probing B_{2u} (Fig. 1), B_{3u} (Fig. 2A) and A_g (Fig. 2B)

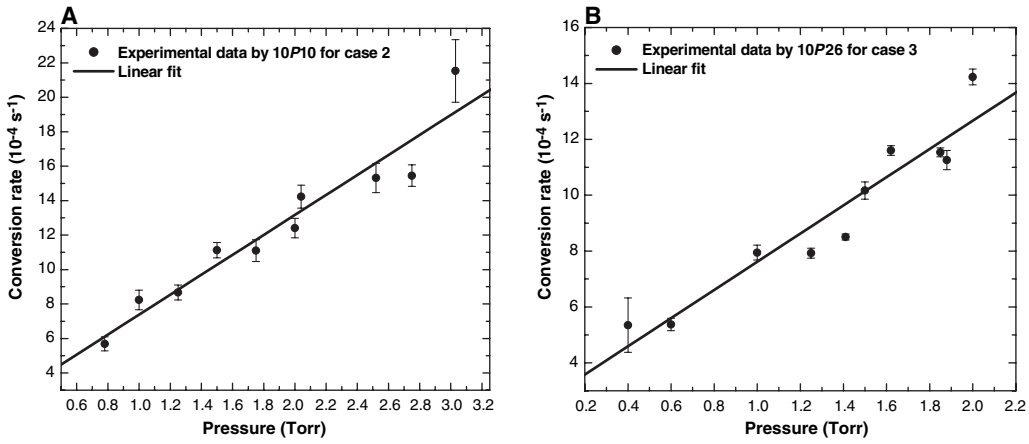

Fig. 3. Observed conversion rates as a function of pressure for probing (**A**) the B_{2u} species by the 10*P*10 line and (**B**) the B_{3u} species by the 10*P*26 line of probe CO_2 laser.

populations. Very similar signals were also observed for alternative B_{2u} and B_{3u} probe resonances (cases 2 and 3 in Table 2). We tried to monitor the B_{1g} population dynamics but were not successful because the line intensity of the resonant $26_{10,16} \leftarrow 27_{9,18}$ transition was too weak. The signals in the third period show the relaxation due to the conversion among spin isomers. A model function $A \exp(-\gamma t) + B$ (where A is the integrated intensity, γ is the observed conversion rate constant, and B is the baseline offset) was fitted to the decay data of Fig. 1 to give the solid smooth curve shown with a rate constant $\gamma = 8.09\ (\pm 0.10) \times 10^{-4}\ s^{-1}$.

The data clearly show that the concentration of the A_g species is almost constant in time, whereas monoexponential kinetics are observed for recovery of the depleted B_{2u} population and decay of the enriched B_{3u} population. Furthermore, the B_{2u} signal does not return to the original zero-difference baseline, and the B_{3u} signal overshoots the baseline and asymptotically approaches a new equilibrium level. These general phenomena can be qualitatively explained using Curl's theory of state mixing (*19*). We assume that conversion of nuclear spin isomers of C_2H_4 is allowed between the B_{2u} and B_{3u} isomers, and between the A_g and B_{1g} isomers, but forbidden between species of opposite inversion symmetry. Specifically, molecular "doorway" states are posited, between either B_{2u} and B_{3u} or A_g and B_{1g}, that are so close in energy that the weak intramolecular nuclear spin-rotation and spin-spin interactions of C_2H_4 can induce mixing between them. This mixing is interrupted by collisions, which promote interconversion between either the B_{2u} and B_{3u} or the A_g and B_{1g} states, through the quantum relaxation process proposed by Chapovsky for *ortho*- and *para*-CH_3F (*20*). Therefore, the time rate of change of the number density of one species is determined by the net number of doorway transitions within species of like inversion symmetry. The concentrations of the B_{2u} and B_{3u} species relax exponentially toward a common depleted equilibrium level, whereas those of the A_g and B_{1g} species retain their initial enriched level with no large relaxation. Net population is thus transferred from the B_{3u} to the B_{2u} state (reflected in the absorption signal of the B_{2u} population not reaching the zero-difference baseline, and the B_{3u} signal passing the baseline).

From the near-constancy of the signal in the third period of Fig. 2B, it appears that spin isomer conversion between states of opposite inversion symmetry is negligible, as is the impact of molecular collisions with the cell wall over the 30-min time range studied. However, over a longer time frame, it is speculated that these factors could cause eventual reequilibrium of the isomer populations to the initial thermal ratios (zero-difference baseline).

The theory of quantum relaxation in *ortho-para* conversion (*20*) predicts that, at low pressure, the spin conversion rate should vary linearly with the total gas concentration p. Thus, the observed first-order rate constant is $\gamma = kp + y$, and varying the pressure allows extraction of the bimolecular rate constant k. So far, this behavior has been observed for CH_3F (*6*, *7*) and $^{13}C^{12}CH_4$ (*8*). For C_2H_4, we measured more than 100 conversion tracks at different pressures and observation times, probing at each of the four B_{2u} and B_{3u} resonances (Table 2, cases 1 to 4). The mean values of γ are plotted in Fig. 3 as a function of pressure. The data fit reasonably well to a linear pressure dependence. Rate constants from the fits for each probe wavelength agree well within the experimental errors (Table 2) and give an average of $5.5\ (\pm 0.8) \times 10^{-4}\ s^{-1}\ torr^{-1}$.

Thus, our spin conversion observations for C_2H_4 are well accounted for by the model of quantum relaxation. The results provide evidence of the weak intramolecular hyperfine interactions in C_2H_4 and suggest that the conversion mechanism among nuclear spin isomers of polyatomic molecules in general is quantum relaxation with conserved inversion symmetry.

References and Notes

1. L. D. Landau, E. M. Lifshitz, *Quantum Mechanics* (Pergamon, Oxford, ed. 3, 1981).
2. A. Farkas, *Orthohydrogen, Parahydrogen, and Heavy Hydrogen* (Cambridge Univ. Press, London, 1935).
3. H. Kawakita *et al.*, *Science* **294**, 1089 (2001).
4. J. E. Dickens, W. M. Irvine, *Astrophys. J.* **518**, 733 (1999).
5. N. Dello Russo *et al.*, *Astrophys. J.* **621**, 537 (2005).
6. P. L. Chapovsky, *JETP* **70**, 895 (1990).
7. B. Nagels, M. Schuurman, P. L. Chapovsky, L. J. F. Hermans, *Phys. Rev. A* **54**, 2050 (1996).
8. P. L. Chapovsky, J. Cosléou, F. Herlemont, M. Khelkhal, J. Legrand, *Chem. Phys. Lett.* **322**, 424 (2000).
9. G. Peters, B. Schramm, *Chem. Phys. Lett.* **302**, 181 (1999).
10. P. R. Bunker, P. Jensen, *Molecular Symmetry and Spectroscopy* (NRC Research Press, Ottawa, ed. 2, 1998), pp. 407–409.
11. V. I. Tikhonov, A. A. Volkov, *Science* **296**, 2363 (2002).
12. F. Kh. Gel'mukhanov, A. M. Shalagin, *JETP Lett.* **29**, 711 (1979).
13. In Table 1, the A_g species corresponds to all four spins aligned, as well as to the case of no net spin. This species corresponds to the symmetric state with respect to the 180° rotations (or interchanges of H nuclei caused by these rotations) about the *x*, *y*, and *z* axes and belongs to the rotational states with the same symmetry $[(K_a, K_c) = (\text{even, even})]$ because of the Pauli principle. The B_{1g}, B_{2u}, and B_{3u} species correspond to the case for one total spin. The B_{1g} state is symmetric with respect to the 180° rotation about the *z* axis and antisymmetric to the rotations about the *x* and *y* axes, belonging to the rotational state with the same symmetry $[(K_a, K_c) = (\text{odd, even})]$; the B_{2u} and B_{3u} states are symmetric with respect to the 180° rotations about the *y* and *x* axes, respectively, and antisymmetric to those about the other two axes (*x* and *z*; *y* and *z*), respectively, belonging to the rotational states shown in Table 1. The A_g, B_{3g}, B_{2u}, and B_{1u} species of nuclear spin isomers of C_2H_4 given by Bunker and Jensen (*10*) correspond to the A_g, B_{1g}, B_{2u}, and B_{3u} species, respectively, used in this work.
14. G. Herzberg, *Molecular Spectra and Molecular Structure. II. Infrared and Raman Spectra of Polyatomic Molecules* (Van Nostrand Reinhold, New York, 1945).
15. T. Oka, *J. Mol. Spectrosc.* **48**, 503 (1973).
16. See supporting material on *Science* Online.
17. I. Cauuet *et al.*, *J. Mol. Spectrosc.* **139**, 191 (1990).
18. In these measurements, the probe laser was locked to the 4.3-μm Lamb-dip fluorescence signal in an external CO_2 cell via a closed servo feedback loop (*21*). To shift the probe CO_2 laser frequency by 100 or 200 MHz, we used one set (for cases 2 to 4) or two sets in tandem (for case 5) of an acousto-optic modulator (IntraAction AGM-1003A1) and an RF modulator driver (GE-10020), respectively.

19. R. F. Curl Jr., J. V. V. Kasper, K. S. Pitzer, *J. Chem. Phys.* **46**, 3220 (1967).
20. P. L. Chapovsky, *Phys. Rev. A.* **43**, 3624 (1991).
21. Z.-D. Sun, F. Matsushima, S. Tsunekawa, K. Takagi, *J. Opt. Soc. Am. B* **17**, 2068 (2000).
22. We express sincere thanks to P. L. Chapovsky for valuable guidance when he visited our laboratory.

Separation and Conversion Dynamics of Four Nuclear Spin Isomers of Ethylene

Zhen-Dong Sun *et al.*

Science **310**, 1938 (2005);
DOI: 10.1126/science.1120037